The Astrophysical Journal, 867:147 (7pp), 2018 November 10 https://doi.org/10.3847/1538-4357/aae6c3
© 2018. The American Astronomical Society. All rights reserved.

Spectroscopy of the Type Ic Supernova SN 2017iuk Associated with Low-redshift GRB 171205A

J. Wang[1,2], Z. P. Zhu[3,1], D. Xu[1], L. P. Xin[1], J. S. Deng[1,2], Y. L. Qiu[1], P. Qiu[4], H. J. Wang[4], J. B. Zhang[4], and J. Y. Wei[1,2]
[1] Key Laboratory of Space Astronomy and Technology, National Astronomical Observatories, Chinese Academy of Sciences, Beijing 100101, People's Republic of China; wj@bao.ac.cn, dxu@nao.cas.cn
[2] School of Astronomy and Space Science, University of Chinese Academy of Sciences, Beijing, People's Republic of China
[3] School of Physics, Huazhong University of Science and Technology, Wuhan 430074, People's Republic of China; zipei@hust.edu.cn
[4] Key Laboratory of Optical Astronomy, National Astronomical Observatories, Chinese Academy of Sciences, Beijing 100101, People's Republic of China
Received 2018 July 23; revised 2018 October 4; accepted 2018 October 4; published 2018 November 12

Abstract

We here report a spectroscopic monitor for the supernova (SN) SN 2017iuk associated with the long-duration low-luminosity gamma-ray burst (GRB) GRB 171205A at a redshift of 0.037, which is up to now the third GRB–SN event away from us. Our spectroscopic observations and spectral analysis allow us to identify SN 2017iuk as a typical broad-line Type Ic SN. A comparison study suggests that the Type IcBL SN 2017iuk resembles SN 2006aj in the following aspects: (1) similar spectra at the nearby epochs, (2) comparable evolution of the photospheric velocity obtained from the measurements based on both the Si II λ6355 line and spectral modeling, and (3) comparable explosion parameters. This analogy could imply the formation of a neutron star in the core collapse of GRB 171205A/SN 2017iuk as previously suggested in GRB 060218/SN 2006aj. The properties of the host galaxy are discussed, which suggest that GRB 171205A/SN 2017iuk occurred in an early-type (S0), high-mass, star-forming galaxy with low specific star formation rate and solar metallicity.

Key words: gamma-ray burst: individual (GRB 171205A) – methods: observational – supernovae: individual (SN 2017iuk) – techniques: spectroscopic

1. Introduction

The connection between long-duration gamma-ray bursts (LGRBs) and their associated broad-line Type Ic supernovae (SN IcBL) with an absolute magnitude of $M_V \sim -19$ mag has been firmly established over the past two decades owing to the prompt spectroscopic follow-up observations (see reviews in Woosley & Bloom 2006; Hjorth & Bloom 2012; Cano et al. 2017 and references therein). So far, the GRB–SN association has been identified in about 30 events with a redshift range from 0.00867 (GRB 980425/SN 1998bw; e.g., Galama et al. 1998) to 1.0585 (GRB 000911; e.g., Lazzati et al. 2001; Masetti et al. 2005), although a nonassociation was firmly identified in two low-z cases: GRB 060505 and GRB 060614 by deep imaging (Della Valle et al. 2006; Fynbo et al. 2006; Gal-Yam et al. 2006).

Study of the SNe associated with LGRBs is important for exploring the nature of death of massive stars. Even though it is widely accepted that LGRBs originate from core collapse of young massive stars (e.g., Woosley & Bloom 2006; Hjorth & Bloom 2012; Wang et al. 2018 and references therein), the compact objects formed in the core collapse are still under hot debate. They could be either a stellar-mass black hole (e.g., Woosley 1993; MacFadyen & Woosley 1999) or a magentar (i.e., a rapidly rotating neutron star with extremely large magnetic field, e.g., Dai & Lu 1998; Woosley & Heger 2006; Bucciantini et al. 2007; Kasen & Bildsten 2010; Zhang & Dai 2010; Mazzali et al. 2014; Wang et al. 2017). In fact, the SN explosion mechanism depends on the compact objects formed in the core collapse. For instance, two types of central engines, i.e., (1) radioactive heating caused by the radioactive decay of nickel and cobalt and (2) rotation energy of a magentar, have been proposed for the powering of the SNe associated with LGRBs (e.g., Iwamoto et al. 2000; Nakamura et al. 2001; Maeda et al. 2003; Greiner et al. 2015; Metzger et al. 2015; Wang et al. 2015; Bersten et al. 2016; Cano et al. 2016, 2017; Dai et al. 2016; Sukhbold et al. 2016).

Among the identified LGRB–SN events, only two cases, i.e., GRB 980425/SN 1998bw and GRB 060218/SN 2006aj (e.g., Mazzali et al. 2006; Pian et al. 2006), are found to be at redshift less than 0.05 (~200 Mpc). Both them can be classified as low-luminosity GRBs (LLGRBs) with an isotropic γ-ray luminosity of $\log L_{\gamma,\rm iso} < 48.5$. In this paper, we report a spectroscopic study for the Type IcBL SN 2017iuk associated with GRB 171205A at a redshift of 0.037, which is up to now the third GRB–SN event away from us.

The paper is organized as follows. Section 2 summarizes the basic properties of GRB 171205A/SN 2017iuk. The spectroscopic observations and data reductions of SN 2017iuk are presented in Section 3. Section 4 shows the analysis and results. A conclusion and implications are presented in Section 5. A ΛCDM cosmology with parameters $H_0 = 70$ km s^{-1} Mpc^{-1}, $\Omega_m = 0.3$, and $\Omega_\Lambda = 0.7$ is adopted throughout the paper.

2. GRB 171205A and Associated SN 2017iuk

GRB 171205A was detected by the *Swift* Burst Alert Telescope (BAT) on 2017 December 05 at 07:20:43 UT (*Swift* trigger 794972; D'Elia et al. 2017a). *Swift* XRT detected a bright new X-ray source at 144.7 s after the BAT trigger (D'Elia et al. 2017b). The BAT on-ground analysis (Barthelmy et al. 2017) reported a duration of $T_{90} = 189.4 \pm 35.0$s, a fluence of $(3.6 \pm 0.3) \times 10^{-6}$ erg cm^{-2} in the 15–150 keV band , and a power-law spectrum with a photon index of $\Gamma = 1.41 \pm 0.14$. A photon index of $\Gamma = 1.717^{+0.035}_{-0.024}$ within the 0.3–10 keV band was reported by a refined XRT analysis (Kennea et al. 2017). The burst was also detected by Konus-*Wind* with a well-fitted power-law spectrum with a $\Gamma = 2.0 \pm 0.14$ in the 20–1500 keV band

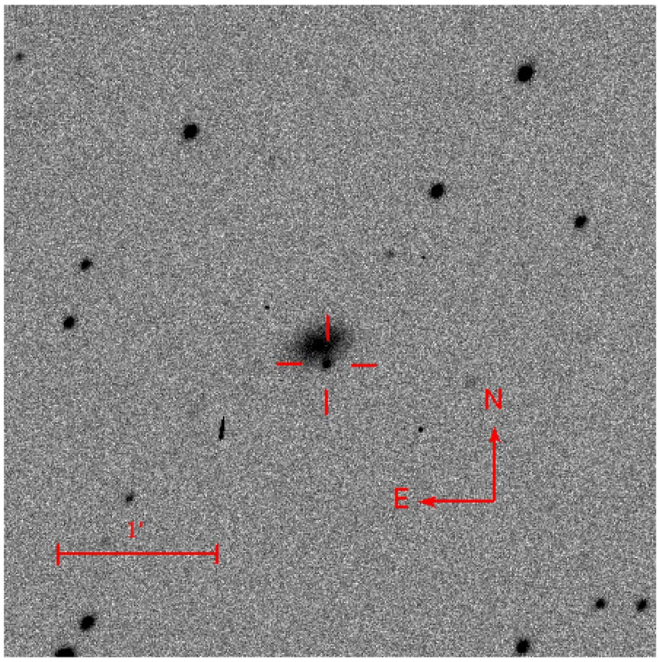

Figure 1. *R*-band image of GRB 171205A/SN 2017iuk and its host galaxy 2MASX J11093966-1235116, which was taken at 2017 December 28, i.e., +23 days after the trigger of the GRB. North is up, and east is to the left. The angular scale of the image is shown in the lower left corner. The burst, marked by the red cross, occurs at the outskirts of the host.

(Frederiks et al. 2017). The reported fluence of $(7.8 \pm 1.6) \times 10^{-6}$ erg cm^{-2} corresponds to an isotropic energy of $E_{\rm iso} \sim 6.6 \times 10^{49}$ erg in the 1–10,000 keV band and to a $\log L_{\gamma,\rm iso} = 47.5$, which allows us to classify GRB 171205A as an LLGRB.

The afterglow of GRB 171205A was observed in multiple wavelengths from near-ultraviolet (NUV) to radio (e.g., Butler et al. 2017; Choi et al. 2017; Cobb 2017; de Ugarte Postigo et al. 2017b; Izzo et al. 2017; Laskar et al. 2017; Mao et al. 2017a, 2017b; Melandri et al. 2017; Perley et al. 2017; Smith & Tanvir 2017). The spectroscopic observation performed by the Very Large Telescope at 1.5 hr after the trigger detected an optical transient at the position R.A.(J2000) = $11^{\rm h}09^{\rm m}39\overset{\rm s}{.}573$ and decl.(J2000) = $-12°35'17\overset{''}{.}37$, which is at the outskirts of the galaxy 2MASX J11093966-1235116 with a redshift of 0.037. The spectrum shows evident Hα, [N II] λ6583, and [S II] $\lambda\lambda$6716, 6731 emission lines at the same redshift of the galaxy. The detection of an associated SN (SN 2017iuk) was reported in 2017 December 07 by a follow-up spectroscopic observation using the 10.4 m GTC telescope (de Ugarte Postigo et al. 2017a). The SN spectrum at that epoch is reported to be similar to the very early spectra of SN 1998bw, which is further confirmed in Prentice et al. (2017).

3. Observations and Data Reductions

Our spectroscopic observations and data reductions are described in this section.

3.1. Observations

The long-slit spectra of GRB 171205A/SN 2017iuk were obtained by the NAOC 2.16 m telescope at Xinglong Observatory (Fan et al. 2016) at five epochs, i.e., December 17, 21, 25, 28, and 30. Figure 1 shows the *R*-band image of the field of GRB 171205A taken by the 2.16 m telescope at 2017 December 28. Our spectroscopic observations were carried out with the Beijing Faint Object Spectrograph and Camera (BFOSC) equipped with a back-illuminated E2V55-30 AIMO CCD as the detector. The grating G4 and a slit of width $1\overset{''}{.}8$ oriented in the south–north direction were used in all five observation runs. This setup finally results in a spectral resolution of ~10 Å, as measured from the sky emission lines and comparison arcs, and provides a wavelength coverage from 3850 to 8000 Å. Except for the observation run at 2017 December 21, the target was observed twice in succession in each run. The exposure time of each frame ranges from 1800 to 4800 s, depending on both the brightness of the object and weather conditions. In each run, the wavelength calibration and flux calibration were carried out by the iron-argon comparison arcs and by the Kitt Peak National Observatory (KPNO) standard stars (Massey et al. 1988), respectively. The spectra of the standard stars were observed with the same instrumental setups immediately after the exposure of the object.

3.2. Data Reductions

Standard procedures were adopted to reduce the 2D spectra by using the IRAF package.[5] The data reduction includes bias subtraction, flat-field correction, and image combination along with cosmic-ray removal before the extraction of the 1D spectra.[6] The contamination due to the underlying host galaxy was taken into account in our extraction through background subtraction. In order to reproduce the gradient of the surface brightness profile of the host, the level of the underlying background is determined by a linear fitting in the two selected background regions. All the extracted 1D spectra were then calibrated in wavelength and flux by the corresponding comparison arc and standards. The flux calibration was performed by comparing the observed spectra of the standards with the spectrophtometrically calibrated spectra provided in the IRAF package, which corrects the specific response of both telescope and spectrograph and the extinction due to Earth's atmosphere. The A-band telluric feature around $\lambda\lambda$7600–7630 due to O_2 molecules was removed from each observed spectrum by the corresponding standard. The Galactic extinction was corrected by the extinction magnitude of $A_{\rm V} = 0.138$ (Schlafly & Finkbeiner 2011) taken from the NASA/IAPC Extragalactic Database (NED), assuming the $R_{\rm V} = 3.1$ extinction law of our Galaxy (Cardelli et al. 1989). The spectra were then transformed to the rest frame, along with the correction of the relativity effect on the flux, according to the redshift of 0.037 of the host galaxy.

4. Analysis and Results

4.1. Identification and Evolution

Figure 2 shows the spectral evolution of SN 2017iuk in the period from +12 to +30 days. The first spectrum taken at +12 days after the onset of the GRB is very blue and featureless, except for the notch at ~6000 Å caused by the Si II λ6355 absorption feature and the two peaks around 4500 and 5300 Å.

[5] IRAF is distributed by the National Optical Astronomical Observatories, which are operated by the Association of Universities for Research in Astronomy, Inc., under cooperative agreement with the National Science Foundation.

[6] The image combination is skipped for the spectrum taken at 2017 December 21 since there was only one exposure. The cosmic-ray removal was performed on the single exposure before spectral extraction.

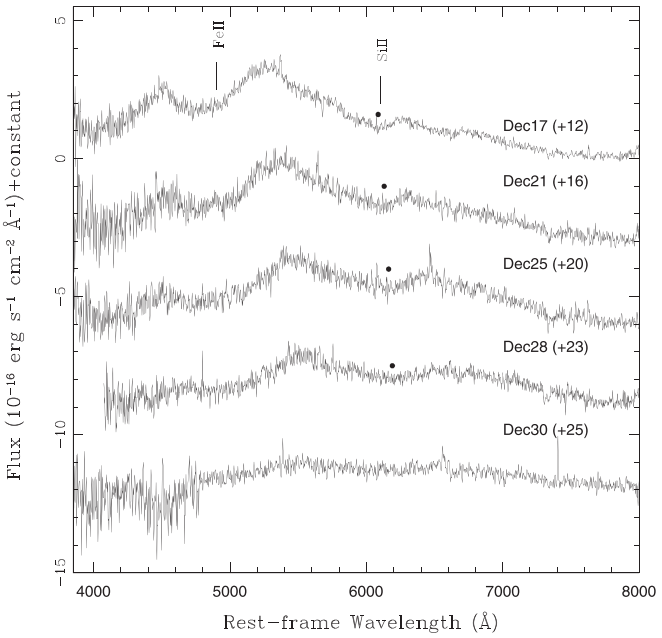

Figure 2. Spectroscopic time series of Type IcBL SN 2017iuk at the five different epochs from 2017 December 17 to 30. All the spectra are transformed to the rest frame based on the redshift of 0.037 and are shifted vertically by an arbitrary amount for visibility. The Fe II λ5169 and Si II λ6355 absorption features are marked on the first spectrum. The black circles show the evolution of the position of the Si II λ6355 absorption.

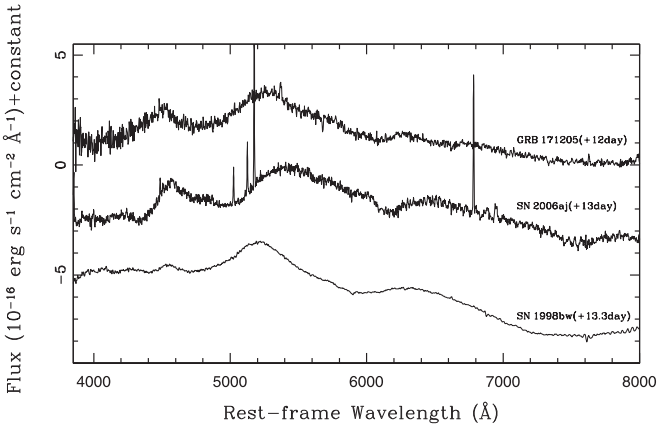

Figure 3. Comparison of the spectrum of SN 2017iuk taken at 2017 December 17 (+12 days) to those of SN 1998bw (+13.3 days) and SN 2006aj (+13.0 days) at similar epochs.

Table 1.
Photospheric Velocities and Blackbody Temperatures Measured from the Spectra

Date	v_{ph}(Si II)	v_{ph}(syn)	T_{bb}
	km s^{-1}	km s^{-1}	K
(1)	(2)	(3)	(4)
2017 Dec 17	12,700 ± 1100	12,000 ± 1000	12,000
2017 Dec 21	10,600 ± 1000	10,000 ± 1000	8000
2017 Dec 25	10,300 ± 1800	10,000 ± 2000	6000
2017 Dec 28	7800 ± 2000	...	...

The latter two features resulted from the Fe II λ5169 absorption (e.g., Filippenko 1997). All these features are quite typical for other GRB–SN events (e.g., D'Elia et al. 2015; Cano et al. 2017), which allows us to classify SN 2017iuk as an SN IcBL with a highly stripped progenitor.

One can see from Figure 2 that the two peaks at ~4500 and ~5300 Å gradually weaken from +12 to 23 days, along with a gradual redshift for the ~5300 Å feature. The bottom spectrum shows that the emission from SN 2017iuk fades out at +30 days, in which there are the marginal ~5300 Å feature and the extremely weak [O I] $\lambda\lambda$6300, 6363 broad emission that is commonly detected in the nebular phase (e.g., Filippenko 1997).

Figure 3 compares the spectrum of SN 2017iuk taken at 2017 December 17 (+12 days), which is close to the *R*-band light peak (X. G. Wang et al. 2018, private communication), to the spectra of SN 1998bw and SN 2006aj at similar epochs. Our comparison clearly suggests an analogy between SN 2017iuk and SN 2006aj.

4.2. Photospheric Velocity

The photospheric expansion velocity in SNe Ibc is traditionally estimated from the Fe II lines at ~5000 Å, because, compared to the Fe II lines, the other ones are produced far above the photosphere. However, this method is unavailable for SNe IcBL owing to their high velocities that result in a line identification difficulty because of the heavy line blending.

We here attempt to estimate photospheric velocity of SN 2017iuk by using the absorption trough of the Si II λ6355 line (e.g., Sahu et al. 2018), except for the last spectrum taken at 2017 December 30. In the last spectrum, the Si II λ6355 feature is too weak to be measured. We mark the positions of the Si II λ6355 line by circles in Figure 2, which clearly shows an evolution of the expansion of the photosphere with a gradually decreasing velocity. The Si II-based photospheric velocities (see Column (2) in Table 1) decrease from 12,000 to 8000 km s^{-1} in the period from +12 to +23 days. This temporal evolution of photospheric velocity is compared to the photospheric velocities of other SNe Ic measured from the Si II line in Figure 4. One can again identify an analogy to SN 2006aj from the evolution of photospheric velocity.

4.3. Spectral Modeling with SYN++

In this section, we model the spectra of SN 2017iuk through the synthetic spectra generated by the SYN++ code (Thomas et al. 2011), which is an enhanced version of the parameterized SN spectrum synthesis code SYNOW (Branch et al. 2000; Fisher 2000). In generating synthetic spectra, the exciting temperature is fixed to be 6000 K, and the involved ions include Fe II, Co II, Si II, Ca II, Mg II, and O I. Based on the synthetic spectra, we fit the observed rest-frame spectra over the whole spectroscopic wavelength range through "chi-by-eye" by changing the blackbody temperature, the optical depth of each ion, and the velocity of the photosphere. The fittings are schemed in Figure 5 for the spectra taken at 2017 December 17, 21, and 25. One can see from the figure that in all three cases the generated synthetic spectra generally match the observed ones quite well, except for the "blue wing" of the ~5000 Å feature. This failure of reproducing might be due to the imperfections of the adopted atomic data of iron, especially when the photospheric temperature is low. The best-fitted photospheric velocities decrease from 12,000 to 10,000 km s^{-1} within the period from +12 to +20 days after the trigger of the

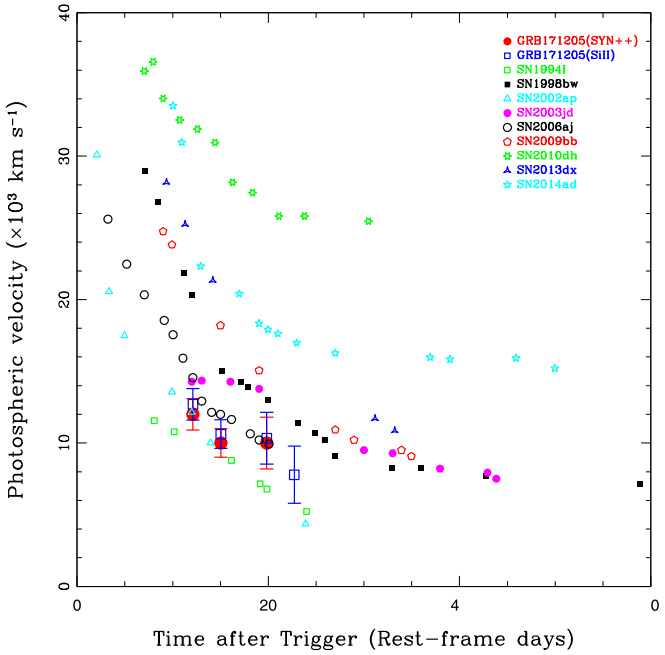

Figure 4. Temporal evolution of the photospheric velocity of SN 2017iuk. The blue open squares mark the photospheric velocities measured from the Si II λ6355 absorption feature, and the red filled circles mark the velocities obtained from the fitting based on the synthetic spectra generated by SYN++. The temporal evolutions of photospheric velocities of other SNe Ic measured from the Si II λ6355 features are plotted for comparison. The data are taken from Sahu et al. (2018).

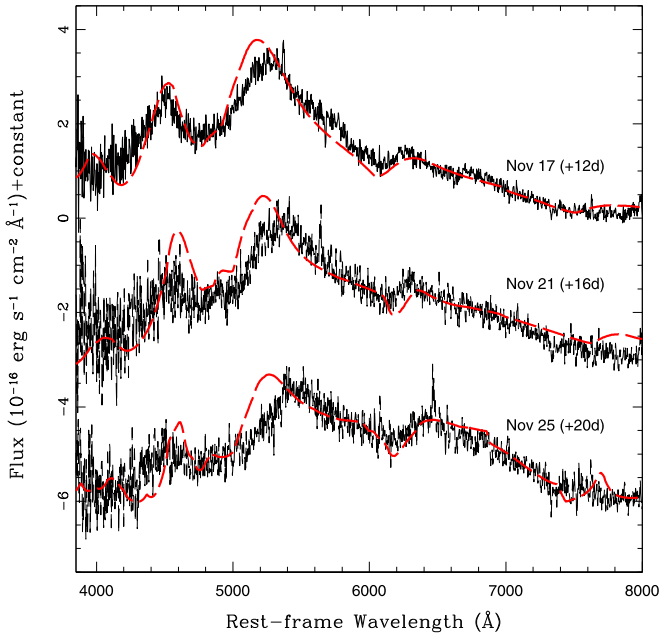

Figure 5. Illustration of the spectral fitting based on the synthetic spectra generated by using SYN++.

GRB. The best-fitted velocities are overplotted in Figure 4, which shows a significant consistency with the measurements based on the Si II absorption. In the period, the modeled blackbody temperatures decrease from 12,000 to 6000 K. The modeled photospheric velocities and blackbody temperatures are tabulated in Table 1 (Columns (3) and (4)).

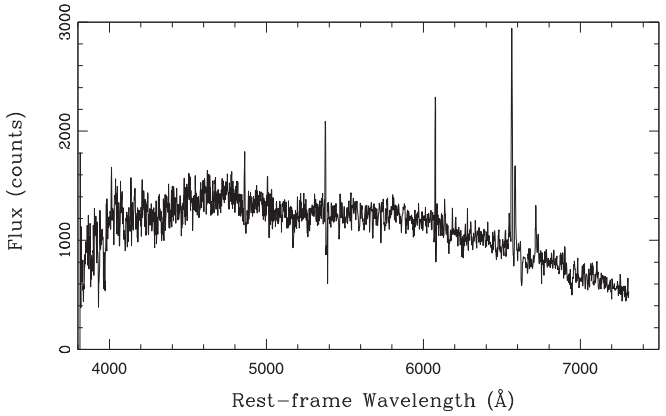

Figure 6. Rest-frame spectrum of the nucleus of the host galaxy of GRB 171205A/SN 2017iuk taken by the 6dF Galaxy Survey. Note that the spectrum lacks absolute flux calibration.

5. Conclusion and Discussion

We monitored SN 2017iuk associated with the LLGRB GRB 171205A in spectroscopy, which is up to now the third GRB–SN event away from us. Our spectroscopy observations and spectral analysis enable us to identify the SN as a broad-line SN Ic. A comparison study suggests that SN 2017iuk resembles SN 2006aj owing to their (1) similar spectra at similar epochs and (2) consistent evolutions of photospheric velocity.

5.1. Explosion Parameters and Mechanism

In this section, we estimate the explosion parameters from our spectral analysis presented in Section 4 and argue that the estimated parameters roughly agree with those of SN 2006aj, which reinforces the analogy revealed in the above section.

We estimate the mass of ejecta $M_{\rm ej}$ from the evolution of photospheric velocity by assuming an exponential density profile $\rho = \rho_0 e^{-\upsilon/\upsilon_e}$, where ρ_0 is the central density and υ_e the e-folding velocity. The evolution of photospheric velocity can be therefore expressed as (Equation (3) in Deng et al. 2001)

$$\upsilon_{\rm ph} \approx -\upsilon_e \ln\left[10^{-6}\frac{\tau_{\rm ph}}{\overline{\kappa}}\left(\frac{\upsilon_e}{10^3\ {\rm km\ s^{-1}}}\right)^2\left(\frac{M_{\rm ej}}{M_\odot}\right)^{-1}\right] - 2\upsilon_e \ln t_{\rm d}, \quad (1)$$

where $\tau_{\rm ph}$ is the optical depth at the photosphere, $\overline{\kappa}$ the optical opacity, and $t_{\rm d}$ the time since explosion in units of days. With the measured $\upsilon_{\rm ph}$, we fitted the evolution of $\upsilon_{\rm ph}$ as $\upsilon_{\rm ph} = a + b \ln t_{\rm d}$. After deriving a value of υ_e from the best-fitted b ($=-2\upsilon_e$), the ejecta mass is inferred to be $M_{\rm ej} \approx 1.1 M_\odot$ from the best-fitted value of a, where the typical values of $\tau_{\rm ph} = 1$ and $\overline{\kappa} = 0.07\ {\rm cm^2\ g^{-1}}$ are adopted in the estimation. The explosion kinetic energy is then estimated to $E_{\rm k} = 6M_{\rm ej}\upsilon_e^2 = 1.4 \times 10^{51}$ erg by integrations of both ρ and $\rho\upsilon^2$ over velocity. Although the inferred $M_{\rm ej}$ and $E_{\rm k}$ are within the ranges of the typical values of SNe IcBL, they are at the lower end of the distributions of the GRB-associated SNe IcBL that have the typical values of $M_{\rm ej} \sim 1$–$10\ M_\odot$ and $E_{\rm k} \sim 1 \times 10^{52}$ erg (e.g., Cano et al. 2017).

We alternatively estimate $E_{\rm k}$ by using the expression of $E_{\rm k} = 3/10 M_{\rm ej}\upsilon_{\rm ph}^2$ given in Arnett (1982, 1996). The photospheric velocity at the time of bolometric maximum, i.e., +12

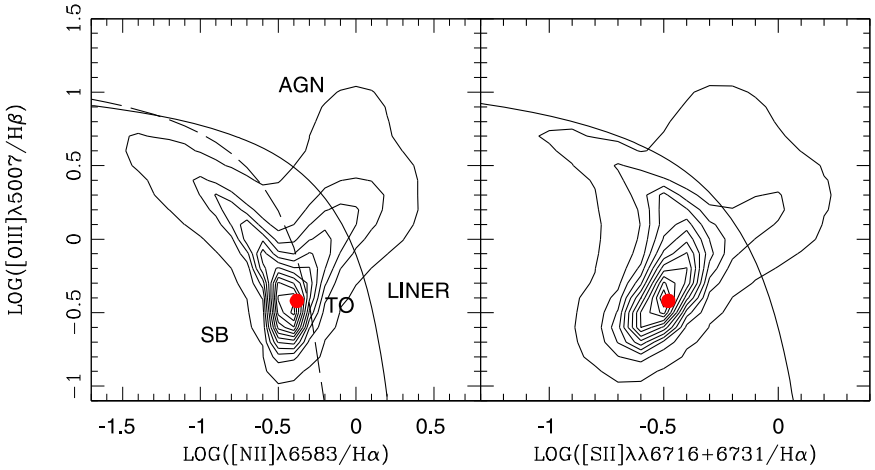

Figure 7. Two BPT diagnostic diagrams for the host galaxy of GRB 171205A/SN 2017iuk. The location of the burst is marked by the red circle in both panels, where the density contours are shown for a typical distribution of the narrow-line galaxies described in Heckman et al. (2004) and Kauffmann et al. (2003). Only the galaxies with signal-to-noise ratio > 20 and the emission lines detected with at least 3σ significance are plotted. The solid lines in both panels mark the theoretical demarcation lines separating AGNs from star-forming galaxies proposed by Kewley et al. (2001). The long-dashed line in the left panel shows the empirical demarcation line proposed in Kauffmann et al. (2003), which is used to separate "pure" star-forming galaxies.

days after the trigger, results in a value of $E_{\rm k} \approx 9 \times 10^{50}$ erg, which is roughly consistent with the above value that is estimated from υ_e. The resulting $E_{\rm k}/M_{\rm ej}$ is $\sim$0.13 for SN 2017iuk.

We argue that the explosion parameters estimated above are comparable to those of SN 2006aj (see Table 3 in Cano et al. 2017). The comparable explosion parameters and the revealed similarity in the spectral evolution motivate us to suspect that SN 2017iuk/GRB 171205A has a similar explosion mechanism to SN 2006aj/GRB 060218. By a detailed modeling of the light curve and spectra, Mazzali et al. (2006) suggested that SN 2006aj/GRB 060218 is produced by a core collapse of a massive star with an initial mass of $\sim 20\,M_\odot$, which expects the formation of a neutron star rather than a black hole after the core collapse.

5.2. Host Galaxy

The host galaxy 2MASX J11093966-1235116 (LCRS B110709.2-121854) of GRB 171205A/SN 2017iuk is classified as an S0 galaxy in the Lyon Extragalactic Database (LEDA). The poor seeing (2.″5–3″) of our observations, however, prevents us from further morphological study on the galaxy. We estimate the total stellar mass ($M_\star$) of the galaxy from its K-band photometry, because the near-infrared emission traces the mass of late-type stars better and is much less sensitive to extinction by dust. With the distance modulus of $\mu = 35.90 \pm 0.15$ mag, the absolute magnitude in K_s band is obtained to be -23.57 ± 0.21 mag, which yields a luminosity in K_s band of $L_K = 5.5 \times 10^{10}\,L_\odot$ by adopting an absolute solar K_s-band magnitude of 3.29 (Blanton & Roweis 2007). Adopting a universal K_s-band mass-to-light ratio $M/L = 0.6$ (Bell & de Jong 2000) finally returns $M_\star = 3.3 \times 10^{10}\,M_\odot$, which is above the average stellar mass of the hosts of nearby LGRBs (e.g., Kruhler et al. 2015; Schulze et al. 2015; Perley et al. 2016)

The spectrum of the nucleus of the host galaxy has been taken by the 6dF Galaxy Survey (Jones et al. 2004), which is a spectroscopic survey using the UK Schmidt telescope at the Anglo-Australian Observatory. The use of robotic positioning optical fibers allows the telescope to measure distances for more than 100,000 galaxies in 6 yr. The rest-frame spectrum[7] extracted from the final data release (DR3; Jones et al. 2009) is shown in Figure 6. It is noted that the spectrum shown in the figure lacks absolute flux calibration. Nevertheless, the spectrum clearly shows that the host galaxy of GRB 171205A is a typical star-forming galaxy with strong Hα, Hβ, [N II] $\lambda\lambda$6548, 6583, and [S II] $\lambda\lambda$6727, 6731 and weak [O III] $\lambda\lambda$4959, 5007 emission lines. Figure 7 shows the occupation on the two empirical Baldwin–Phillips–Terlevich (BPT) diagrams for the host galaxy. The diagrams, which were originally proposed by Baldwin et al. (1981) and then refined by Veilleux & Osterbrock (1987), are traditionally used as a powerful tool to determine the dominant energy source in emission-line galaxies according to their emission-line ratios. By measuring the flux of each emission line through direct integration, the figure shows that the host galaxy is located within the locus of the star-forming sequence very well.

We then estimate the star formation rate (SFR) from its NUV detection. The brightness at the NUV band (peaked at $\sim$2300 Å) of *GALEX* is reported to be 18.12 ± 0.04 mag. At the beginning, the NUV brightness is corrected for the Milky Way dust extinction from color excess through $A_{\rm NUV} = R_{\rm NUV} E(B-V)$. The parameter $R_{\rm NUV}$ is determined to be 6.62 (Fitzpatrick 1999) and updated to be 7.24 ± 0.08 by Yuan et al. (2013). The calibration of SFR $= 1 \times 10^{-28} L_{\rm NUV}\,M_\odot\,{\rm yr}^{-1}$, obtained by converting the relation from Kennicutt (1998) to the initial mass function in Kroupa (2001), is used to estimate the SFR, where $L_{\rm NUV}$ is the NUV luminosity in units of erg s^{-1}. With the extinction-corrected NUV brightness, we finally obtain an SFR of $\sim 1\,M_\odot\,{\rm yr}^{-1}$ for the host galaxy of GRB 171205A/SN 2017iuk, which is larger than the average value of the host galaxies of LGRBs at a similar redshift (e.g., Kruhler et al. 2015). With the estimated stellar mass of the host, the specific SFR (sSFR), defined as the SFR normalized to the total stellar mass, is inferred to be as low as $\sim 0.03\,{\rm Gyr}^{-1}$. In fact, this value is at the lower end of the distribution of sSFR of samples of LGRB hosts

[7] The rest-frame spectrum is transformed from the observed one by applying both Galactic extinction and Doppler corrections. See Section 3.2.2 for a detailed description.

(e.g., Savaglio et al. 2009; Japelj et al. 2016). Assuming a constant SFR over the growth history of the host, the growth timescale $t_\star = M_\star/\mathrm{SFR}$ is estimated to be about 30 Gyr. This timescale is comparable to (or larger than) the Hubble time of the local universe, which implies a quiescent growth of the host galaxy of SN 2017iuk/GRB 171205A.

We finally estimate nuclear metallicity of the host galaxy of GRB 171205A/SN 2017iuk from the spectrum. The oxygen metallicity is simply calculated from the $N2$ method proposed in Pettini & Pagel (2004): $12 + \log(\mathrm{O/H}) = 8.90 + 0.57N2$, where $N2 = \log([\mathrm{N\,II}]/\mathrm{H}\alpha)$, because the $[\mathrm{N\,II}]/\mathrm{H}\alpha$ line ratio is insensitive to both flux calibration and intrinsic dust extinction. The metallicity of the galaxy is inferred to be $12 + \log(\mathrm{O/H}) = 8.69$, which equals the solar gas-phase value (Allende Prieto et al. 2001; Asplund et al. 2004). In fact, by using a strong-line diagnostic, Kruhler et al. (2015) reported that the oxygen metallicities range from 7.0 to 9.0 for a sample of 44 LGRBs within a redshift range from 0.3 to 3.4.

In summary, GRB 171205A/SN 2017iuk occurred in an early-type, high-mass, star-forming galaxy with low sSFR and solar metallicity.

The authors thank the anonymous referee for a careful review and helpful suggestions that improved the manuscript. The study is supported by the National Basic Research Program of China (grant 2014CB845800) and by the Strategic Pioneer Program on Space Science, Chinese Academy of Sciences, grant no. XDA15052600. J.W. is supported by the National Natural Science Foundation of China under grants 11473036 and 11773036. D.X. acknowledges the support by the One-Hundred-Talent Program of the Chinese Academy of Sciences (CAS), by the Strategic Priority Research Program Multi-wavelength Gravitational Wave Universe of the CAS (no. XDB23000000), and by the National Natural Science Foundation of China under grant 11533003. Special thanks go to the staff at Xinglong Observatory as a part of National Astronomical Observatories, China Academy of Sciences, for their instrumental and observational help, and to the allocated observers who allowed us to finish the observations in ToO mode. This study is partially supported by the Open Project Program of the Key Laboratory of Optical Astronomy, NAOC, CAS. The study uses the data collected by 6dF Galaxy Survey, which was carried out by the staff of the Australian Astronomical Observatory.

Facility: Xinglong Observatory 2.16 m telescope.

Software: IRAF (Tody 1986, 1993), SYN++ (Thomas et al. 2011), SYNOW (Branch et al. 2000; Fisher 2000).

ORCID iDs

J. Wang https://orcid.org/0000-0002-6880-4481

References

Allende Prieto, C., Barklem, P. S., Asplund, M., & Ruiz Cobo, B. 2001, ApJ, 558, 830
Arnett, W. D. 1982, ApJ, 253, 785
Arnett, W. D. 1996, Supernovae and Nucleosynthesis: An Investigation of the History of Matter from the Big Bang to the Present (Princeton, NJ: Princeton Univ. Press)
Asplund, M., Grevesse, N., Sauval, A. J., Allende Prieto, C., & Kiselman, D. 2004, A&A, 417, 751
Baldwin, J. A., Phillips, M. M., & Terlevich, R. 1981, PASP, 93, 5
Barthelmy, S. D., Cummings, J. R., D'Elia, V., et al. 2017, GCN, 22184, 1
Bell, E. F., & de Jong, R. S. 2000, MNRAS, 312, 497
Bersten, M. C., Benvenuto, O. G., Orellana, M., & Nomoto, K. 2016, ApJL, 817, 8
Blanton, M. R., & Roweis, S. 2007, AJ, 133, 734
Branch, D., Jeffery, D. J., Blaylock, M., & Hatano, K. 2000, PASP, 112, 217
Bucciantini, N., Quataert, E., Arons, J., Metzger, B. D., & Thompson, T. A. 2007, MNRAS, 380, 1541
Butler, N., Watson, A. M., Kutyrev, A., et al. 2017, GCN, 22182, 1
Cano, Z., Johansson, A. K. G., Maeda, K., et al. 2016, MNRAS, 457, 2761
Cano, Z., Wang, S. Q., Dai, Z. G., & Wu, X. 2017, AdAst, 2017, 8929054
Cardelli, J. A., Clayton, G. C., & Mathis, J. S. 1989, ApJ, 345, 245
Choi, C., Im, M., Gak, L. S., et al. 2017, GCN, 22188, 1
Cobb, B. E. 2017, GCN, 22270, 1
Dai, Z. G., & Lu, T. 1998, PhRvL, 81, 4301
Dai, Z. G., Wang, S. Q., Wang, J. S., Wang, L. J., & Yu, Y. W. 2016, ApJ, 817, 132
D'Elia, V., D'Ai, A., Lien, A. Y., & Sbarufatti, B. 2017a, GCN, 22177, 1
D'Elia, V., D'Ai, A., Melandri, A., et al. 2017b, GCN, 22271, 1
D'Elia, V., Pian, E., Melandri, A., et al. 2015, A&A, 577, 116
de Ugarte Postigo, A., Izzo, L., Kann, D. A., et al. 2017a, ATel, 11038, 1
de Ugarte Postigo, A., Schulze, S., Bremer, M., et al. 2017b, GCN, 22187, 1
Della Valle, M., Chincarini, G., Panagia, N., et al. 2006, Natur, 444, 1050
Deng, J., Qiu, Y. L., & Hu, J. Y. 2001, arXiv:astro-ph/0106404
Fan, Z., Wang, H. J., Jiang, X. J., et al. 2016, PASP, 128, 115005
Filippenko, A. V. 1997, ARA&A, 35, 309
Fisher, A. K. 2000, PhD thesis, Univ. Oklahoma
Fitzpatrick, E. L. 1999, PASP, 111, 63
Frederiks, D., Golenetskii, S., Aptekar, R., et al. 2017, GCN, 22227, 1
Fynbo, J. P. U., Watson, D., Thone, C. C., et al. 2006, Natur, 444, 1047
Galama, T. J., Vreeswijk, P. M., van Paradijs, J., et al. 1998, Natur, 395, 670
Gal-Yam, A., Fox, D. B., Price, P. A., et al. 2006, Natur, 444, 1053
Greiner, J., Mazzali, P. A., Kann, D., et al. 2015, Natur, 523, 189
Heckman, T. M., Kauffmann, G., Brinchmann, J., et al. 2004, ApJ, 613, 109
Hjorth, J., & Bloom, J. S. 2012, in Gamma-Ray Bursts, Vol. 51 ed. C. Kouveliotou, R. A. M. J. Wijers, & S. Woosley (Cambridge: Cambridge Univ. Press), 169
Iwamoto, K., Nakamura, T., Nomoto, K., et al. 2000, ApJ, 534, 660
Izzo, L., Selsing, J., Japelj, J., et al. 2017, GCN, 22180, 1
Japelj, J., Vergani, S. D., Salvaterra, R., et al. 2016, A&A, 590, 129
Jones, D. H., Read, M. A., Saunders, W., et al. 2009, MNRAS, 399, 683
Jones, D. H., Saunders, W., Colless, M., et al. 2004, MNRAS, 355, 747
Kasen, D., & Bildsten, L. 2010, ApJ, 717, 245
Kauffmann, G., Heckman, T. M., Tremonti, C., et al. 2003, MNRAS, 346, 1055
Kennea, J. A., Sbarufatti, B., Burrows, D. N., et al. 2017, GCN, 22183, 1
Kennicutt, R. C., Jr. 1998, ARA&A, 36, 189
Kewley, L. J., Dopita, M. A., Sutherland, R. S., Heisler, C. A., & Trevena, J. 2001, ApJ, 556, 121
Kroupa, P. 2001, MNRAS, 322, 231
Kruhler, T., Malesani, D., Fynbo, J. P. U., et al. 2015, A&A, 581, 125
Laskar, T., Coppejans, D. L., Margutti, R., & Alexander, K. D. 2017, GCN, 22216, 1
Lazzati, D., Covino, S., Ghisellini, G., et al. 2001, A&A, 378, 996
MacFadyen, A. I., & Woosley, S. E. 1999, ApJ, 524, 262
Maeda, K., Mazzali, P. A., Deng, J. S., et al. 2003, ApJ, 593, 931
Mao, J., Ding, X., & Bai, J.-M. 2017a, GCN, 22186, 1
Mao, J., Ding, X., & Bai, J.-M. 2017b, GCN, 22195, 1
Masetti, N., Palazzi, E., Pian, E., et al. 2005, A&A, 438, 841
Massey, P., Strobel, K., Barnes, J. V., et al. 1988, ApJ, 328, 315
Mazzali, P. A., Deng, J., Nomoto, K., et al. 2006, Natur, 442, 1018
Mazzali, P. A., McFadyen, A. I., Woosley, S. E., Pian, E., & Tanaka, M. 2014, MNRAS, 443, 67
Melandri, A., D'Avanzo, P., di Fabrizio, L., Padilla, C., & D'Elia, V. 2017, GCN, 22189, 1
Metzger, B. D., Margalit, B., Kasen, D., & Quataert, E. 2015, MNRAS, 454, 3311
Nakamura, T., Mazzali, P. A., Nomoto, K., & Iwamoto, K. 2001, ApJ, 550, 991
Perley, D. A., Schulze, S., & de Ugarte Postigo, A. 2017, GCN, 22252, 1
Perley, D. A., Tanvir, N. R., Hjorth, J., et al. 2016, ApJ, 817, 8
Pettini, M., & Pagel, B. E. J. 2004, MNRAS, 348, L59
Pian, E., Mazzali, P. A., Masetti, N., et al. 2006, Natur, 442, 1011
Prentice, S., Mazzali, P., Smartt, S. J., et al. 2017, ATel, 11060, 1
Sahu, D. K., Anupama, G. C., Chakradhari, N. K., et al. 2018, MNRAS, 475, 2591
Savaglio, S., Glazebrook, K., & Le Borgne, D. 2009, ApJ, 691, 182
Schlafly, E. F., & Finkbeiner, D. P. 2011, ApJ, 737, 103
Schulze, S., Chapman, R., Hjorth, J., et al. 2015, ApJ, 808, 73
Smith, I. A., & Tanvir, N. R. 2017, GCN, 22242, 1

Sukhbold, T., Ertl, T., Woosley, S. E., Brown, J. M., & Janka, H.-T. 2016, ApJ, 821, 38
Thomas, R. C., Nugent, P. E., & Meza, J. C. 2011, PASP, 123, 237
Tody, D. 1986, Proc. SPIE, 627, 733
Tody, D. 1993, in ASP Conf. Ser. 52, Astronomical Data Analysis Software and Systems II, ed. R. J. Hanisch, R. J. V. Brissenden, & J. Barnes (San Francisco, CA: ASP), 173
Veilleux, S., & Osterbrock, D. E. 1987, ApJS, 63, 295
Wang, J., Xin, L. P., Qiu, Y. L., Xu, D. W., & Wei, J. Y. 2018, ApJ, 855, 91
Wang, L. J., Yu, H., Liu, L. D., et al. 2017, ApJ, 837, 128
Wang, S. Q., Wang, L. J., Dai, Z. G., & Wu, X. F. 2015, ApJ, 799, 107
Woosley, S. E. 1993, ApJ, 405, 273
Woosley, S. E., & Bloom, J. S. 2006, ARA&A, 44, 507
Woosley, S. E., & Heger, A. 2006, ApJ, 637, 914
Yuan, H. B., Liu, X. W., & Xiang, M. S. 2013, MNRAS, 430, 2188
Zhang, B., & Dai, Z. G. 2010, ApJ, 718, 841